Astronomy & Astrophysics

Hot ammonia in NGC 6334I & I(N)[*]

H. Beuther[1], A. J. Walsh[2], S. Thorwirth[3], Q. Zhang[4], T. R. Hunter[5], S. T. Megeath[6], and K. M. Menten[3]

[1] Max-Planck-Institut für Astronomie, Königstuhl 17, 69117 Heidelberg, Germany
   e-mail: beuther@mpia.de
[2] James Cook University, Townsville, QLD 4811, Australia
   e-mail: Andrew.Walsh@jcu.edu.au
[3] Max-Planck-Institut für Radioastronomie, Auf dem Hügel 69, 53121 Bonn, Germany
   e-mail: sthorwirth@mpifr-bonn.mpg.de
[4] Harvard-Smithsonian Center for Astrophysics, 60 Garden Street, Cambridge, MA 02138, USA
   e-mail: zhang@cfa.harvard.edu
[5] NRAO, 520 Edgemont Rd, Charlottesville, VA 22903, USA
   e-mail: thunter@nrao.edu
[6] Ritter Observatory, Department of Physics and Astronomy, University of Toledo, Toledo, OH 43606-3390, USA
   e-mail: megeath@astro1.panet.utoledo.edu

ABSTRACT

Aims. The massive twin cores NGC 6334I and I(N) are in different evolutionary stages and hence ideal targets to study evolutionary variations within the same larger-scale environment. Here, we study the warm, compact gas components.

Methods. We imaged the two regions with the Australia Telescope Compact Array (ATCA) at high angular resolution in the $NH_3(3, 3)$ to (6, 6) inversion lines.

Results. Compact emission is detected toward both regions in all observed inversion lines with energy levels up to 407 K above ground. This is particularly surprising for NGC 6334I(N) since it lacks bright infrared emission and is considered a massive cold core at an early evolutionary stage. High optical depth and multiply-peaked line profiles complicate rotation temperature estimates, and we can only conclude that gas components with temperatures >100 K are present in both regions. Toward NGC 6334I, we confirm previous reports of $NH_3(3, 3)$ maser emission toward the outflow bow-shocks. Furthermore, we report the first detection of an $NH_3(6, 6)$ maser toward the central region of NGC 6334I. This maser is centered on the second millimeter (mm) peak and elongated along the outflow axis, indicating that this mm continuum core harbors the driving source of the molecular outflow. Toward the main mm peak in NGC 6334I(N), we detect a double-horn line profile in the $NH_3(6, 6)$ transition. The current data do not allow us to differentiate whether this double-horn profile is produced by multiple gas components along the line of sight, or whether it may trace a potential underlying massive accretion disk.

Key words. techniques: interferometric – stars: early-type – stars: formation – ISM: individual objects: NGC 6334I and I(N) – line: profiles – masers

1. Introduction

The massive star-forming regions NGC 6334I and I(N) are located at the north-eastern end of the NGC 6334 molecular cloud/HII region complex at an approximate distance of 1.7 kpc in the southern hemisphere (Neckel 1978; Straw & Hyland 1989). The whole NGC 6334 complex has been subject to intense studies in many wavelength bands for more than two decades (e.g., McBreen et al. 1979; Rodríguez et al. 1982; Gezari 1982; Loughran et al. 1986; de Pree et al. 1995; Tapia et al. 1996; Sandell 2000; Carral et al. 2002; Beuther et al. 2005; Hunter et al. 2006).

The region NGC 6334I contains the well known cometary-shaped Ultracompact HII (UCHII) region NGC 6334F and associated molecular gas and dust emission. Various maser types were found, from H_2O masers (Moran & Rodríguez 1980; Forster & Caswell 1989) and OH masers (Gaume & Mutel 1987;

Brooks & Whiteoak 2001) to Class II CH_3OH maser emission (Norris et al. 1993; Caswell 1997; Walsh et al. 1998). Furthermore, mid-infrared imaging has identified a potential exciting star for the UCHII region (De Buizer et al. 2002). The main molecular gas and dust peaks are located at the north-western edge of the UCHII region (e.g., Kraemer & Jackson 1995; Beuther et al. 2005; Hunter et al. 2006). Multi-frequency submillimeter (submm) and millimeter (mm) dust continuum imaging indicates dust temperatures of the order 100 K (Sandell 2000). Single-dish molecular line surveys revealed a rich line forest (e.g., McCutcheon et al. 2000; Thorwirth et al. 2003; Schilke et al. 2006) comparable to those observed toward hot core regions like Orion-KL. A molecular outflow has been observed with a velocity range of approximately 150 km s^{-1} (Bachiller & Cernicharo 1990; Leurini et al. 2006). $NH_3(3, 3)$ maser as well as shocked H_2 emission was reported toward the end of the outflow lobes (Kraemer & Jackson 1995; Davis & Eisloeffel 1995; Persi et al. 1996; Megeath & Tieftrunk 1999).

The source NGC 6334I(N) is located approximately 2′ to the north of NGC 6334I. It also exhibits strong (sub)mm continuum emission but at lower temperatures (~30 K). Molecular

line surveys of NGC 6334I(N) revealed that most species exhibit fainter emission than that found toward NGC 6334I, although there are some species like HC_3N which are stronger in NGC 6334I(N) (Megeath & Tieftrunk 1999; McCutcheon et al. 2000; Thorwirth et al. 2003; Sollins & Megeath 2004). No mid-infrared and only weak near-infrared emission has been detected toward NGC 6334I(N) by Tapia et al. (1996). Recent deeper near-infrared imaging has found evidence for a cluster of low-mass stars in this region (Persi et al. 2005). Carral et al. (2002) report the detection of two faint cm continuum sources, one of them associated with Class II CH_3OH maser emission (Caswell 1997; Walsh et al. 1998). Furthermore, Kogan & Slysh (1998) observed a cluster of Class I CH_3OH masers, and Megeath & Tieftrunk (1999) detected a bipolar outflow in north-west south-east direction in the thermal SiO emission. NGC 6334I(N) is considered to be the younger of the two regions.

To better characterize this intriguing pair of massive star-forming regions, we started an observational campaign with the Australia Telescope Compact Array (ATCA) and the Submillimeter Array (SMA) from centimeter (cm) to submm and mm wavelengths. Beuther et al. (2005) investigated the regions with the ATCA in the $NH_3(1, 1)$ and (2, 2) lines as well as CH_3OH emission near 25 GHz. They found compact hot gas cores in all lines toward NGC 6334I, however, in NGC 6334I(N) only extended NH_3 emission, and no thermal CH_3OH at the observed frequencies, was detected. Toward both regions, the temperatures were too high to derive reasonable rotational temperatures with the low-energy-level NH_3 transitions. Hunter et al. (2006) identified multiple mm continuum sources in both regions (four in NGC 6334I and seven in NGC 6334I(N)). Furthermore, an additional north-east south-west outflow is identified toward NGC 6334I(N) (Hunter et al. in prep.), oriented approximately perpendicular to the one previously reported by Megeath & Tieftrunk (1999).

To get a better understanding of the hot gas components toward the twin cores NGC 6334I and I(N), here we report a follow-up study of the $NH_3(3, 3)$ to (6, 6) inversion lines with the ATCA.

2. Observations

We observed NGC 6334I and I(N) in November 2005 during two nights with the ATCA in the compact 750D configuration, also including antenna 6. This results, at 25 GHz, in projected baselines between 3.8 and 369 kλ. The phase reference centers were RA (J2000) $17^h20^m53^s.44$, Dec (J2000) $-35°47'02''.2$ for NGC 6334I and RA (J2000) $17^h20^m54^s.63$, Dec (J2000) $-35°45'08''.9$ for NGC 6334I(N). We observed the $NH_3(3, 3)$, (4, 4), (5, 5), and (6, 6) inversion lines with the frequencies of the main hyperfine components at 23.870, 24.139, 24.533, and 25.056 GHz, respectively. The velocities relative to the local standard of rest (v_{lsr}) for NGC 6334I and NGC 6334I(N) are ~-7.6 and ~-3.3 km s^{-1}, respectively. Good uv-coverage was obtained through regular switching between both sources and the four spectral setups. On-source integration times for each of the $NH_3(3, 3)$ and (4, 4) lines, in both sources, were 220 min. The (5, 5) and (6, 6) lines were observed each for 200 min in NGC 6334I and for 190 min in NGC 6334I(N). The spectral resolution of the observations was 62 kHz, corresponding to a velocity resolution of ~0.8 km s^{-1}. The primary beam of the ATCA at the given frequency is $\sim130''$. The data were reduced with the MIRIAD package. Applying a robust weighting of 1 (closer to natural than uniform weighting, thus stressing the shorter

baselines) the synthesized beam is $1.9'' \times 1.1''$. The rms per 1 km s^{-1} channel is ~3 mJy.

3. Results

The four observed NH_3 inversion lines cover a broad range of energy levels above ground with lower energy levels E_1 between 123 and 407 K ($E_1(NH_3(3, 3)) = 123$ K, $E_1(NH_3(4, 4)) = 200$ K, $E_1(NH_3(5, 5)) = 295$ K, $E_1(NH_3(6, 6)) = 407$ K). The previous $NH_3(1, 1)$ and (2, 2) data of Beuther et al. (2005) extend the range of observed energy levels down to 23 K. Hence, we are able to trace various temperature components throughout the two star-forming regions. All 6 inversion lines up to $NH_3(6, 6)$ were detected in both target regions (Figs. 1 and 2). While this is less surprising for NGC 6334I, the northern source NGC 6334I(N) lacks strong infrared emission and is considered a prototypical massive cold core at a very early stage of star formation (e.g., Gezari 1982). While it is still considered to be a very young source, the detection of the high energy level transitions up to $NH_3(6, 6)$ clearly shows that compact warm gas components already exist at this early evolutionary stage. We discuss both regions separately first.

3.1. NGC 6334I

3.1.1. Hot thermal NH_3 emission

The uv-spectra taken on the shortest baseline in NGC 6334I (Fig. 1) are rare examples showing even the satellite hyperfine components, in the highly excited $NH_3(5, 5)$ and (6, 6) lines, in emission (~26 and ~31 km s^{-1} offset from the v_{lsr}). Figure 3 presents integrated images of all 6 NH_3 inversion transitions from the (1, 1) to the (6, 6) transition (the (1, 1), (2, 2) and cm continuum images are adapted from Beuther et al. 2005). Except for the (3, 3) line, we show the integrated emission of the main central hyperfine line. Only for the (3, 3) transition we integrated over the two hyperfine components at higher frequencies (negative velocities) because the main line is contaminated by maser emission (see Kraemer & Jackson 1995; and Sect. 3.1.2 below).

The $NH_3(1, 1)$ and (2, 2) maps show two peaks associated with the two main mm continuum sources, mm1 and mm2, reported by Hunter et al. (2006). While the two peaks have approximately the same intensities in the low-energy NH_3 lines, the mm dust continuum flux density of mm1 is approximately 1.5 times higher than that of mm2 (Hunter et al. 2006). The $NH_3(3, 3)$ hyperfine map shows emission toward the north-eastern mm source, mm1, and only weaker emission toward the south-western mm source, mm2. Re-inspecting the $NH_3(1, 1)$ and (2, 2) data, integrated maps of their satellite hyperfine lines are also stronger toward mm1 than toward mm2, although the main hyperfine lines show the same intensities toward both mm peaks. This indicates that the NH_3 optical depth toward mm2 has to be lower than toward mm1. The higher NH_3 inversion lines all show a bright emission peak near mm1, and a much weaker peak near mm2. Particularly in the $NH_3(4, 4)$ and (5, 5) lines, this weaker peak is shifted to the west of mm2 toward the mid-infrared source detected by De Buizer et al. (2002). Although in the lower energy NH_3 lines the two mm peaks appear similar, the fact that the higher energy lines are much stronger toward mm1 indicates that this is the warmer of two sources.

One of the aims of this study is to get temperature estimates of the warm gas. We identify the positions of the two main molecular line peaks with the $NH_3(6, 6)$ emission peak (RA (J2000) 17:20:53.42, Dec (J2000) $-35:46:57.7$, offset
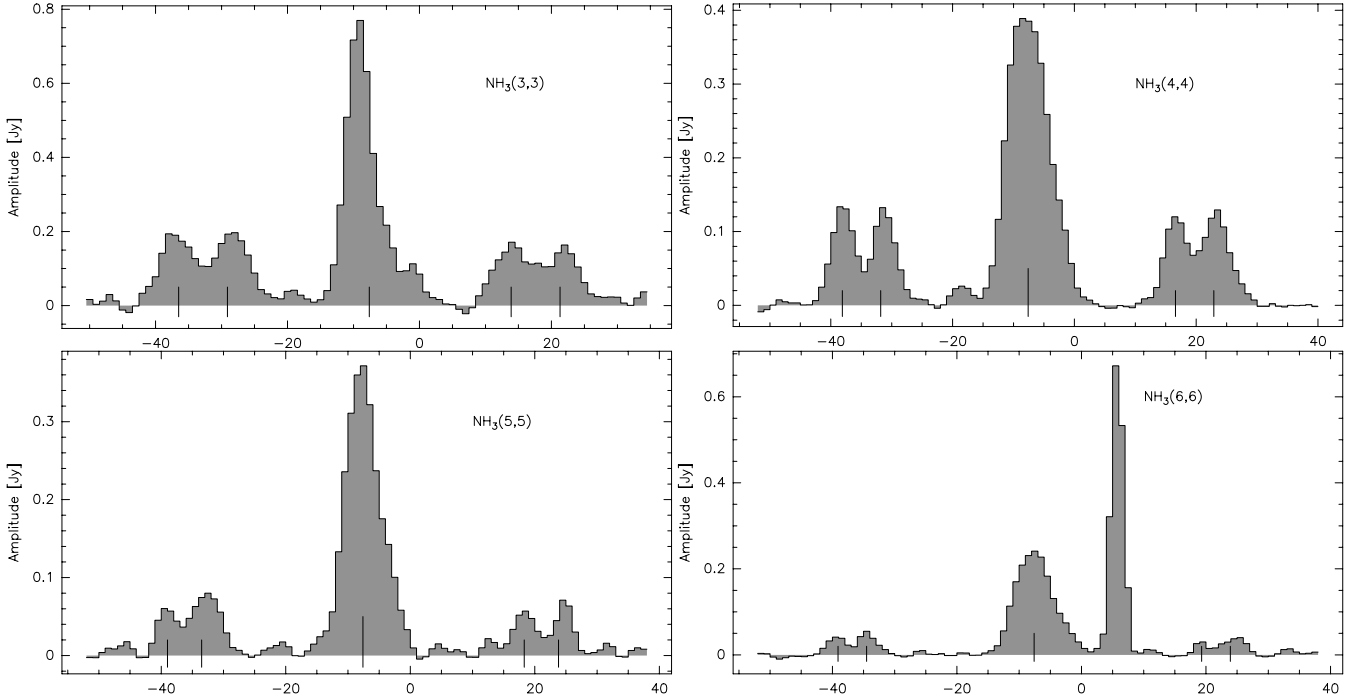
Fig. 1. UV-Spectra of the NH_3 inversion lines on the shortest baseline toward NGC 6334I. The lines mark the spectral positions of the main and satellite hyperfine components.
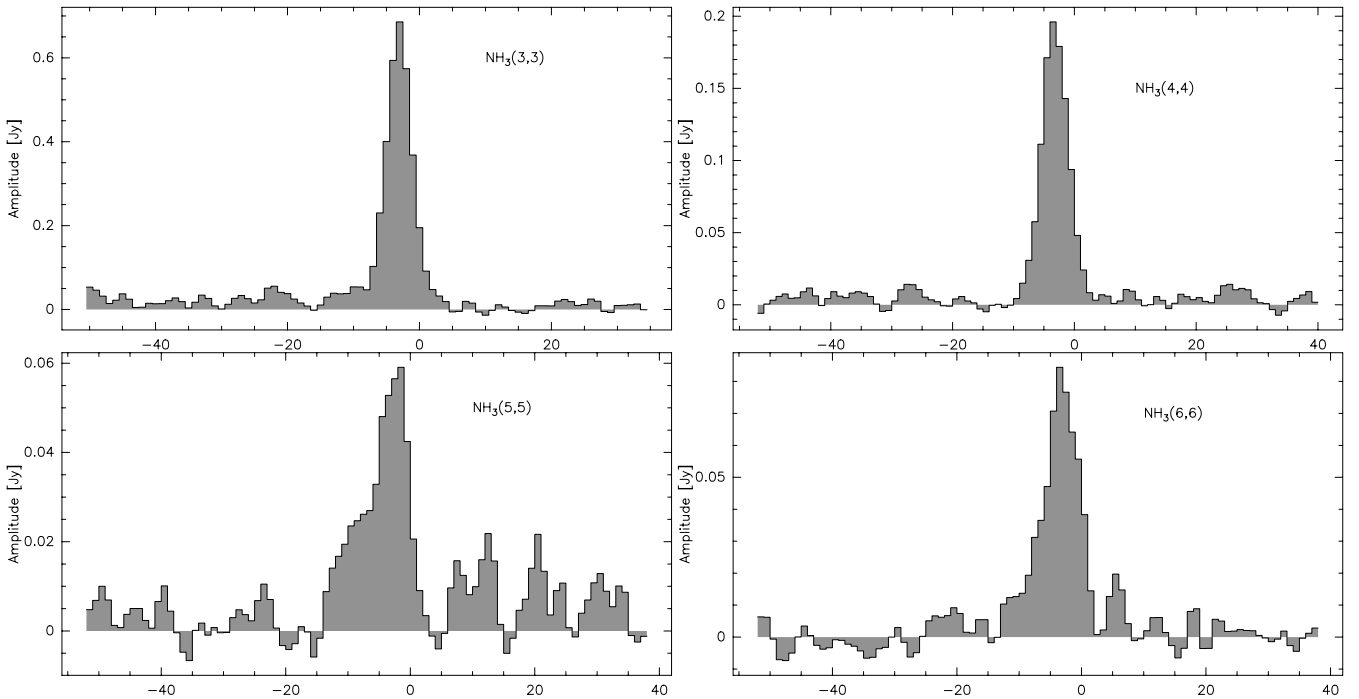

Fig. 2. UV-spectra of the NH_3 inversion lines on the shortest baseline toward NGC 6334I(N).

$-0.3''/4.5''$ from the phase center) near mm1, and one Class II CH_3OH maser feature (RA (J2000) 17:20:53.18, Dec (J2000) -35:46:59.3, Caswell 1997; Walsh et al. 1998, offset $-3.2''/2.9''$ from the phase center) near mm2. The spectra of all four newly observed lines toward these two positions are presented in Fig. 4. Fitting of the hyperfine structure was done in CLASS which is part of the GILDAS software suite[1]. Recent frequency

measurements for NH_3 and its deuterated variants (Coudert & Roueff 2006) have been taken into account.

Toward both positions, the $NH_3(3, 3)$ and $(4, 4)$ lines are optically thick so we are not able to derive reasonable fits with the standard fitting procedures assuming constant excitation temperatures. This way we get only flat-topped synthetic spectra. Since such flat-topped spectra are not observed, this indicates that different temperatures likely exist along the line of sight. The most extreme case is the $NH_3(3, 3)$ spectrum toward NGC 6334I-mm1 (Fig. 4 top-left panel): in the optically thin case the peak
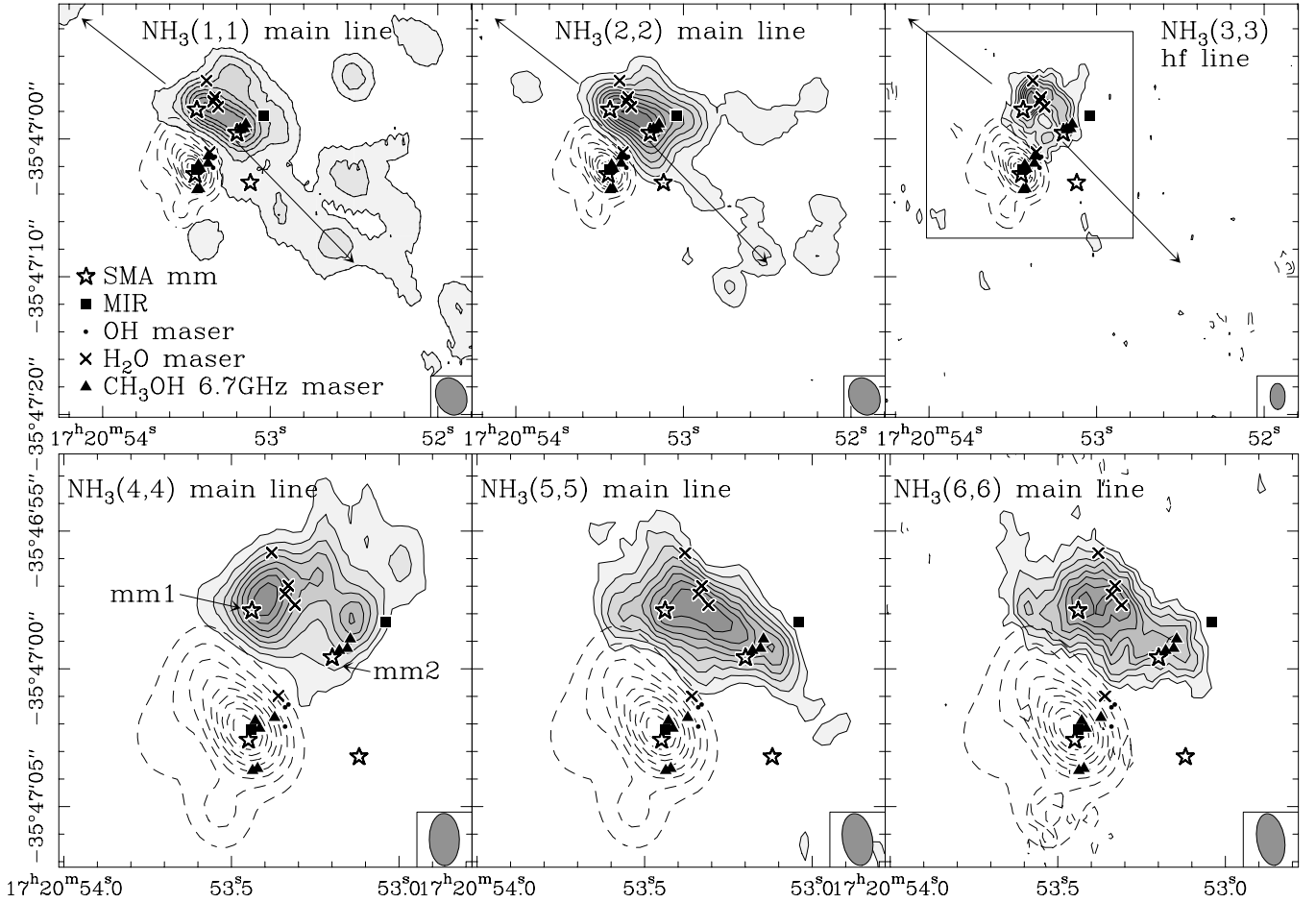

Fig. 3. Integrated NH$_3$ inversion line images of the thermal emission toward NGC 6334I are shown in grey-scale with solid contours. The (1, 1) and (2, 2) images are adapted from Beuther et al. (2005). In all cases we show the integrated main line (see Fig. 1), except for the (3, 3) transition where we present the emission integrated over the two hyperfine satellite components at blue-shifted velocities (see Fig. 1). The top-row images are shown on larger spatial scales than the bottom-row images, the inlay size for the bottom-row images is shown in the (3, 3) panel. The contouring of the (1, 1) and (2, 2) is done in 3σ steps with 3σ values of 21 and 12 mJy beam^{-1}, respectively. The (3, 3) to (6, 6) integrated images are contoured from 20 to 90% (step 10%) of the peak emission with peak values of 22.5, 32.6, 24.2 and 17.5 mJy beam^{-1}, respectively. The dashed contours show the Ultracompact H$_{II}$ region from Beuther et al. (2005), contoured from 10 to 90% (step 10%) of the peak emission of 1197 mJy beam^{-1}. The markers are labeled in the top row, SMA mm continuum emission is from Hunter et al. (2006), H$_2$O maser emission from Forster & Caswell (1989), CH$_3$OH class II maser emission from Walsh et al. (1998), OH maser emission from Brooks & Whiteoak (2001) and MIR sources from De Buizer et al. (2002). The two main mm continuum sources mm1 and mm2 are labeled in the bottom-left panel. The arrows in the top row mark the direction of the CO/SiO outflow. The synthesized beams are shown at the bottom-right of each panel. The data to this figure are available in electronic form at the CDS.

intensities of the satellite hyperfine lines should be 3% of the peak intensity of the main line. However, in this case the satellite hyperfine lines of the NH$_3$(3, 3) transition have more or less the same intensities as the main line, indicating the large optical depth. Since we cannot fit these lines well, we use the higher excitation NH$_3$(5, 5) and (6, 6) lines for the temperature estimates.

Reasonable fits are possible for these two lines, and we measure the peak intensities, the opacities of the main lines, and the line-widths (Table 1). The spectral peak intensities toward these two positions are similar, which is in contrast to the integrated images shown in Fig. 3. However, the line-widths toward mm1 are more than 2 km s^{-1} larger than those toward mm2; this accounts for the differences in the integrated images. Because the NH$_3$(5, 5) and (6, 6) lines are of different NH$_3$ species (para-NH$_3$ and ortho-NH$_3$, respectively), their different statistical weights have to be taken into account. Doing this, we can derive rotational temperatures (T_{rot}) toward the molecular peak positions associated with mm1 and mm2. The derived T_{rot}(55, 66) values are 86 ± 20 K and 67 ± 20 K for the two positions, respectively.

Although the temperatures are comparable within the error-bars, the data are indicative that temperatures associated with mm1 may be higher than those associated with mm2.

For the very optically thick lines where the previous fits failed, it is also possible to estimate approximate opacities τ_{main} from the observed line ratios between the main and the satellite hyperfine components. Following Ho & Townes (1983), we then calculated the rotational temperatures, T_{rot}, and NH$_3$ column densities. Table 2 list the values derived via this approach. The estimated opacities of the (3, 3) and (4, 4) lines are all significantly larger than those we derived from the (5, 5) and (6, 6) lines. Interestingly, the rotational temperature for mm2 corresponds well to the rotational temperature derived from the higher excited line pair above. In contrast to that, the temperature we now derived for mm1 is higher than that derived from the higher excitation lines by a factor of about 1.6. While the estimated errors associated with the the (3, 3)/(4, 4) line pair are even larger than for the (5, 5)/(6, 6) pair, this derivation confirms the previous assessment that mm1 is likely the warmer of the two sources.
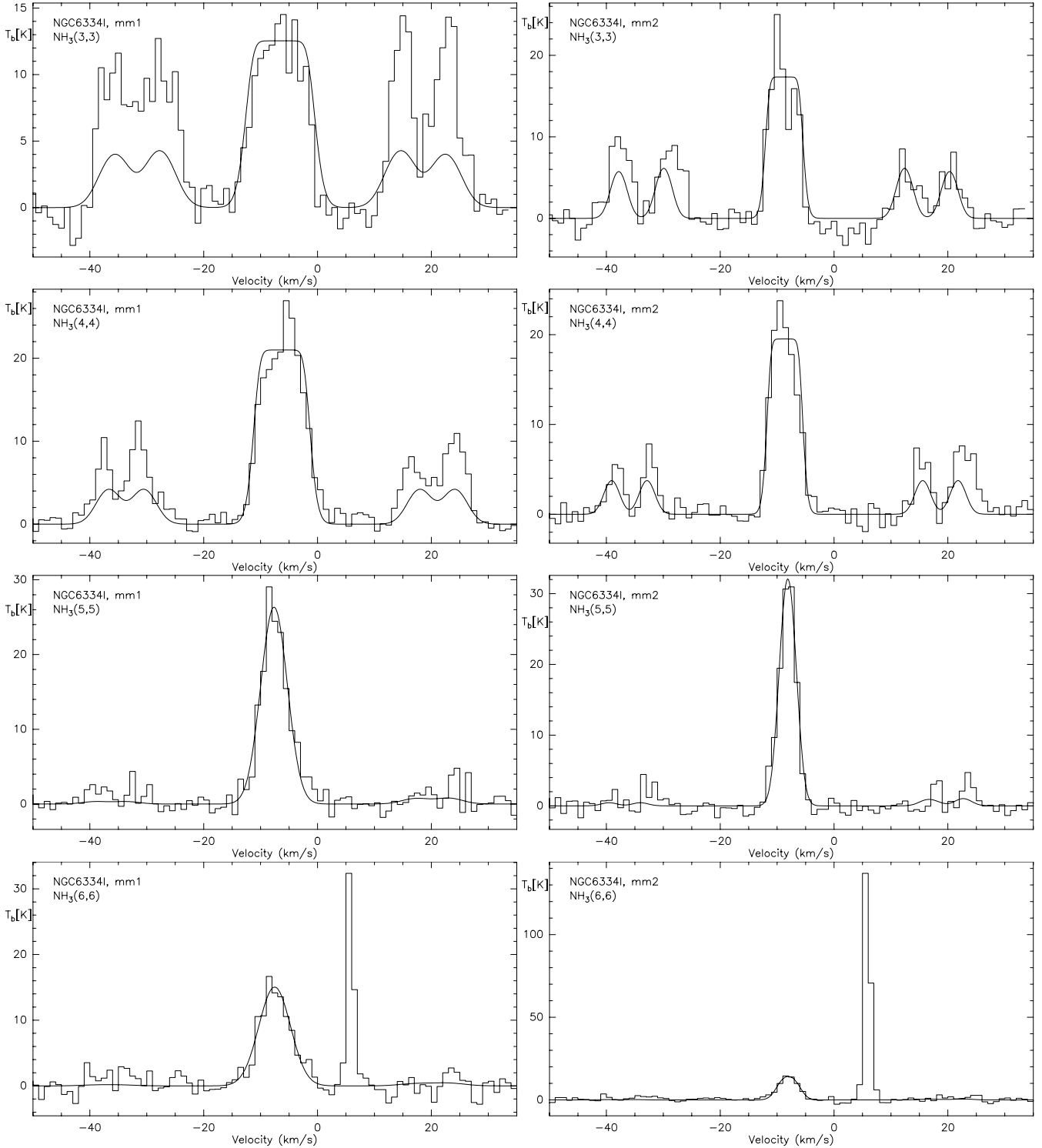
Fig. 4. NH$_3$(3, 3) to (6, 6) spectra toward the molecular peak positions associated with the mm continuum peaks mm1 and mm2. The spectral resolution is smoothed to 1 km s^{-1} and the spatial resolution to 2.8″ × 2.2″ (the same as the spatial resolution of the lower energy lines presented in Beuther et al. 2005). The additional strong peaks at positive velocities in the NH$_3$(6, 6) spectra are a maser discussed in Sect. 3.1.2. The solid lines show fits to the spectra. The (3, 3) and (4, 4) lines are optically thick so that reasonable fits are not possible. The data to this figure are available in electronic form at the CDS.

The NH$_3$ column densities derived this way would correspond to H$_2$ column densities of the order a few times 10^{26} cm^{-2} (assuming NH$_3$ Orion hot core abundances as listed in van Dishoeck & Blake 1998). This is about 1–2 orders of magnitude larger than the H$_2$ column densities one can derive at comparable spatial scales from the mm continuum data (Hunter et al. 2006). This

is an additional indicator of the limitations one has to face when the lines have as high opacities as in the case of NGC 6334I. Future radiative transfer modeling may explain these observed spectral lines better; however, this is beyond the scope of this paper.

Table 1. Fitted parameters and rotational temperatures in NGC 6334I.

	mm1	mm2
Offset ["]	–0.3/4.5	–3.2/2.9
$T_b(NH_3(5, 5))$ [K]	26.4 ± 0.3	32.2 ± 0.3
$\Delta v(NH_3(5, 5))$ [km s^{-1}]	5.4 ± 0.2	3.3 ± 0.2
$v_{peak}(NH_3(5, 5))$ [km s^{-1}]	–7.6 ± 0.1	–8.1 ± 0.1
$\tau_{main}(NH_3(5, 5))^a$	0.1±1.8	0.4 ± 0.5
$T_b(NH_3(6, 6))$ [K]	15.1 ± 0.3	14.3 ± 0.3
$\Delta v(NH_3(6, 6))$ [km s^{-1}]	6.4±0.6	3.5 ± 0.6
$v_{peak}(NH_3(6, 6))$ [km s^{-1}]	–7.5 ± 0.2	–8.0 ± 0.1
$\tau_{main}(NH_3(6, 6))^a$	0.1 ± 2.8	1.4 ± 1.6
$T_{rot}(5, 5/6, 6)^b$ [K]	86 ± 20	67 ± 20

^{a} τ_{main} is prone to the largest errors, since the fits in Fig. 4 do not accurately reproduce the satellite lines. ^{b} The errors for T_{rot} are estimated by varying τ_{main} within errors.

Table 2. Parameters for NGC 6334I derived via the satellite/main line ratios.

	mm1	mm2
Offset ["]	–0.3/4.5	–3.2/2.9
$\tau_{main}(NH_3(3, 3))$	64 ± 5	13 ± 5
$\tau_{main}(NH_3(4, 4))$	28 ± 5	20 ± 5
$T_{rot}(3, 3/4, 4)$ [K]	140 ± 50	70 ± 50
$N(NH_3)^a$ [cm^{-2}]	$1.0 \times 10^{19} \pm 30\%$	$6.8 \times 10^{18} \pm 30\%$

^{a} Since we cannot derive reasonable line-widths for these lines, for the column density calculations we assume $\Delta v = 5.2$ and $\Delta v = 3.2$ for mm1 and mm2, respectively (see Table 1).

The $NH_3(6, 6)$ line-width is larger toward mm1 than the $NH_3(5, 5)$ line-width. For mm2, they are approximately the same within the errorbars. It would be interesting to compare these line-widths also with those of the lower excitation lines. Since, we cannot accurately fit the whole spectra (see Fig. 4), we tried to derive the line widths via Gaussian fits to the satellite hyperfine components. However, for the same transitions, Gaussian fits of various satellite hyperfine components result in different line-widths (differences up to 1 km s^{-1}) indicative of the high optical depth and the complex source structure that is also evident in the various hyperfine components. Therefore, a comparison of the line-widths of the lower-excitation lines is difficult. Nevertheless, toward mm1 the larger line-width of the higher excitation $NH_3(6, 6)$ line compared to $NH_3(5, 5)$ indicates larger internal motions of the warmer gas which is likely closer to the central source.

3.1.2. $NH_3(3, 3)$ and (6, 6) maser emission

Kraemer & Jackson (1995) reported $NH_3(3, 3)$ maser emission toward the outflow lobes in NGC 6334I. This observation is confirmed by our data (Figs. 5 and 6). The most north-eastern (3, 3) maser spot is resolved and shows a morphology expected from bow-shocks in molecular outflows. A Gaussian fit to the spectrum extracted toward the bow-shocks results in a peak-brightness temperature $T_b \sim 160$ K and a linewidth $\Delta v \sim 1.6$ km s^{-1}. The maser emission is identified by a combination of high brightness temperatures, narrow line-widths and peculiar spatial distributions, all with respect to the known thermal gas components. This agrees with the argument set forth by Kraemer & Jackson (1995) that the $NH_3(3, 3)$ maser emission is not associated with any other maser types, but that it is likely caused by shocks when the outflow impinges on the ambient molecular gas.

Here, we report $NH_3(6, 6)$ maser emission toward NGC 6334I (Figs. 4–6). We believe that this is the first detection of $NH_3(6, 6)$ maser emission. The $NH_3(6, 6)$ maser is not associated with the $NH_3(3, 3)$ maser emission toward the outflow lobes, but rather, the (6, 6) maser emission is found at the core center and peaks coincident with the Class II CH_3OH maser group associated with mm2. The maser emission is resolved and elongated in the north-east south-western direction approximately along the large-scale outflow axis. This apparent extended structure is likely a superposition of several point-like sub-features which cannot be resolved by our observations. Weak $NH_3(6, 6)$ maser emission is found in the vicinity of mm1 and associated with the H_2O maser cluster. The v_{lsr} of the (6, 6) maser is +5.8 km s^{-1} approximately 13 km s^{-1} offset from the thermal emission at that position. The FWHM of the maser feature is ~1.3 km s^{-1}, far smaller than the line-width of the thermally excited lines reported in Table 1. The H_2O maser velocities reported by (Forster & Caswell 1989) range from −45.6 to −0.8 km s^{-1} and are hence also offset from the $NH_3(6, 6)$ maser velocity. Although the Class II CH_3OH maser peaks are at the same positions, their velocities (from −6 to −12 km s^{-1}, Walsh et al. 1998) are also offset from the $NH_3(6, 6)$ maser velocity. Unfortunately, from a theoretical point of view, the $NH_3(6, 6)$ maser has not been studied yet, and we thus have no predictions of what to expect. As discussed in Sect. 4.1, the $NH_3(6, 6)$ maser morphology indicates that its emission is associated with the molecular outflow. Although we do not yet understand the peculiar velocity of the (6, 6) maser, this indicates that it is likely associated with some outflow-shock processes. Further theoretical and observational work is required to understand its characteristics in better detail.

3.2. NGC 6334I(N)

One of the surprising results of our previous $NH_3(1, 1)$, (2, 2) and CH_3OH (around 25 GHz) study was the absence of compact molecular line emission toward the main mm continuum peak in NGC 6334I(N) (Beuther et al. 2005). The NH_3 emission of the low excitation lines peaks approximately at the mm continuum position, but it is extremely extended without a clearly peaked morphology indicative of compact gas cores (Fig. 7 reproduces the data from Beuther et al. 2005). Therefore, one of the aims of this new study was to search for compact warm gas components associated with the mm continuum sources, the strongest of which is the mm1 source labeled in Fig. 7. The $NH_3(3, 3)$ emission appears less extended than the (1, 1) and (2, 2) maps but it is still relatively extended and mainly south of the mm continuum peaks. It is spatially associated with neither of the two outflows but rather located between their two southern outflow lobes. Perhaps there is some kind of interaction zone between the two molecular outflows which preferentially excites the $NH_3(3, 3)$ line. However, this is far from clear and we refrain from further interpretation of the $NH_3(3, 3)$ morphology here. Going to the higher excitation lines, the $NH_3(4, 4)$ line is the first transition that shows compact emission close to the mm continuum peaks. However, the emission peak is offset by about two arcseconds to the north-west from the main mm continuum peak, mm1. This may partially be an opacity effect because imaging the satellite hyperfine component at negative velocities – although the peak is weak on a 5σ level – it peaks toward the main mm source mm1. Only the two highest excited lines, $NH_3(5, 5)$ and (6, 6) clearly peak toward the strongest mm peak mm1. Both maps show a secondary peak a few arcseconds south-east associated with mm2. We do not detect any compact
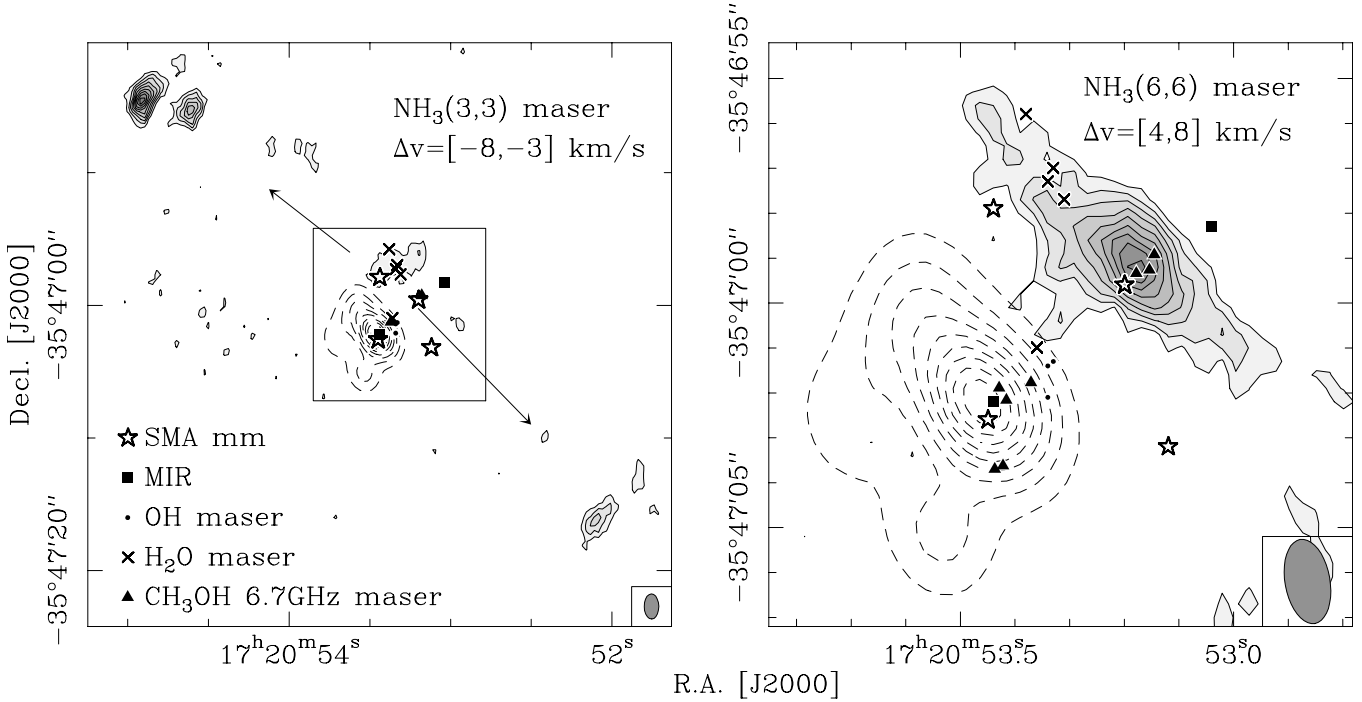
Fig. 5. NH$_3$(3, 3) and (6, 6) maser emission in NGC 6334I is shown in the *left* and *right panel*, respectively. Velocity ranges of integrated emission are given in each panel and the markers are the same as in Fig. 3. The contour levels are from 15 to 95% (step 10%) of the peak emission, which is 112.5 and 126.8 mJy beam^{-1} for the (3, 3) and (6, 6) maser lines. The dashed contours show the Ultracompact HII region from Beuther et al. (2005), contoured from 10 to 90% (step 10%) of the peak emission of 1197 mJy beam^{-1}. The right panel again shows a smaller region as shown by the inlay in the left panel. The synthesized beams are shown at the bottom-right of each panel. The data to this figure are available in electronic form at the CDS.
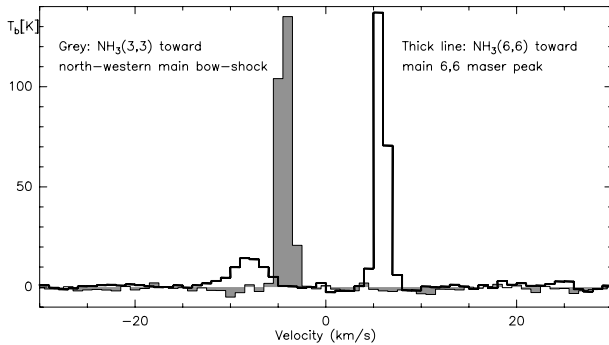

Fig. 6. NH$_3$(3, 3) and (6, 6) maser spectra in grey and thick lines, respectively. The (3, 3) spectrum is extracted toward the main north-eastern bow-shock, and the (6, 6) spectra is taken toward the main (6, 6) maser peak close to mm2. (see Fig. 5). The data to this figure are available in electronic form at the CDS.

NH$_3$ emission toward mm4 which is associated with a cm continuum source and a Class II CH$_3$OH maser (Walsh et al. 1998; Carral et al. 2002; Hunter et al. 2006).

Only the NH$_3$(5, 5) and (6, 6) lines appear reasonable for a temperature estimate toward the main mm continuum and high-excitation NH$_3$ peak, because the NH$_3$(1, 1) and (2, 2) inversion lines trace only extended gas, the (3, 3) line shows the strange emission south of the mm sources, and the (4, 4) line peak is also offset from mm1. Figure 8 presents the NH$_3$(5, 5) and (6, 6) spectra measured toward their main emission peaks toward mm1. While the NH$_3$(5, 5) line shows a relatively simple single-peaked profile, the NH$_3$(6, 6) line shows a double-peaked profile with the two emission peaks separated by approximately ±2 km s^{-1} from the peak-velocity derived from the NH$_3$(5, 5)

profile. With a 1σ rms of the NH$_3$(6, 6) spectrum of 1.36 K, the difference between the emission peak at -1.5 km s^{-1} and the dip at -3.5 km s^{-1} is $\sim$3.4σ. It is not possible to derive a 1 component fit for this (6, 6) profile which could then be used with the (5, 5) spectrum to derive a temperature estimate similar to the case in NGC 6334I. Therefore, we refrain from a rotational temperature estimate here, however, kinetic temperatures in excess of 100 K are needed to explain the detection of the highly excited NH$_3$(5, 5) and (6, 6) lines.

4. Discussion

4.1. The outflow driving source in NGC 6334I

What is the driving source of the large-scale north-east south-west outflow in NGC 6334I first reported by Bachiller & Cernicharo (1990) and later confirmed by Kraemer & Jackson (1995) and Hunter et al. (2006)?

The larger line-widths observed toward mm1 compared to mm2 indicate more internal motion toward mm1 – either turbulent motion or organized motion due to infall, outflow or rotation. Furthermore, the fact that the highest excitation lines preferentially peak on the strongest mm continuum source mm1 indicates that this is the warmest source and potentially the strongest power house of the region, which would favor that source as the driving source of the outflow. However, mm line and continuum observations with the Submillimeter Array (Hunter et al. in prep.) show that mm2 has a higher line to continuum ratio and that mm1 and mm2 are equally bright in several CH$_3$OH lines with energy levels above ground of a few 100 K. Therefore, we cannot unambiguously conclude whether mm1 is the warmer source or not. Furthermore, the NH$_3$(6, 6) maser peak is clearly associated with the mm continuum source
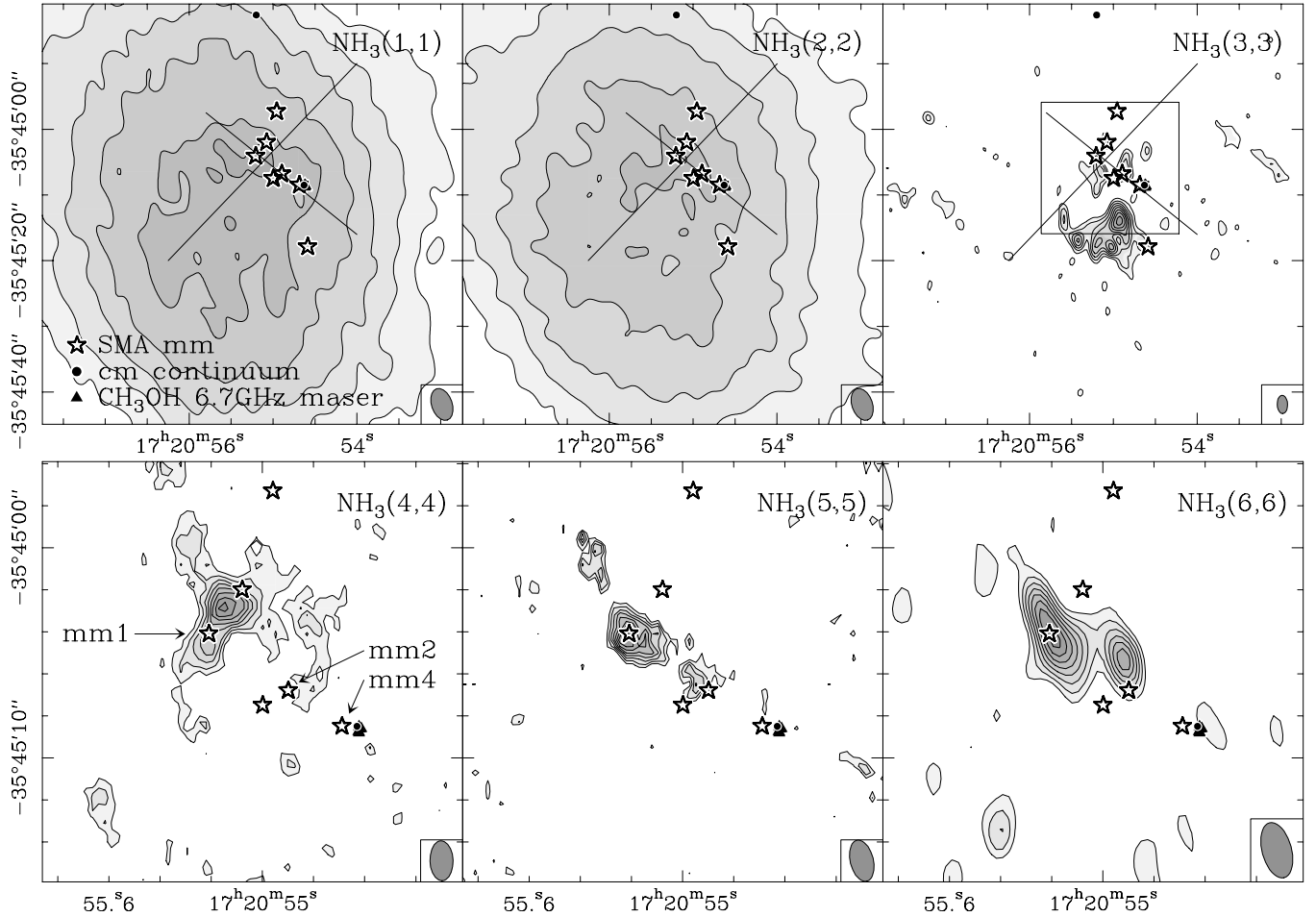
Fig. 7. Integrated main hyperfine component NH$_3$ inversion line images of the thermal emission toward NGC 6334I(N) are shown in grey-scale with solid contours. The (1, 1) and (2, 2) images are adapted from Beuther et al. (2005). The *top-row images* are shown on larger spatial scales than the *bottom-row images*, the inlay size for the *bottom-row images* is shown in the (3, 3) panel. The contour levels are 58(58)348 mJy/beam and 33(33)198 mJy/beam for the NH$_3$(1, 1) and (2, 2) lines, respectively. The (3, 3) to (6, 6) integrated images are contoured from 25 to 95% (step 10%) of the peak emission with peak values of 12.9, 11.6, 10.0 and 10.0 mJy beam^{-1}, respectively. The markers are labeled in the top row, SMA mm continuum emission is from Hunter et al. (subm.), CH$_3$OH class II maser emission from Walsh et al. (1998) and the cm continuum emission from Carral et al. (2002). The mm continuum sources mm1, mm2 and mm4 from Hunter et al. (2006) are labeled in the *bottom-left panel*. The large cross indicates the two main axis of the two identified molecular outflows. The synthesized beams are shown at the bottom-right of each panel. The data to this figure are available in electronic form at the CDS.

mm2, and the position angle (PA) of the elongation of the maser (6, 6) feature is ∼48° from north, comparable to the PA of the CO outflow of ∼46° (Bachiller & Cernicharo 1990). This same orientation of the (6, 6) maser elongation with the large-scale molecular outflow indicates that the maser emission may be produced by shock interaction of the outflow with the ambient core gas close to the driving sources (in contrast to the NH$_3$(3, 3) maser features further outside). Therefore, we suggest that this secondary mm source, mm2, may be the driving source of the strong high-velocity molecular outflow.

4.2. Double-peaked NH$_3$(6, 6) emission in NGC 6334I(N)

The double-peaked NH$_3$(6, 6) profile toward the main mm continuum peak in NGC 6334I(N) is peculiar and requires further consideration. In typical infall studies, usually an optically thin and an optically thick line are observed, and if the optically thick line shows an absorption dip with a blue-red asymmetry at the velocity of the peak emission of the optically thin line, this is a first indicator of potential infall motion (e.g., Myers et al. 1996).

Fitting the NH$_3$(5, 5) spectrum shown in Fig. 8, the optical depth of the main hyperfine component is of order unity. Although NH$_3$(6, 6) is part of the statistically favored ortho-NH$_3$ (its statistical weight is double that of para-NH$_3$), and we cannot precisely determine the optical depth of this higher excitation (6, 6) line from its double-peaked profile, it is unlikely to be very much larger than that of the (5, 5) line. Therefore, a typical infall interpretation appears unlikely.

Another possibility to produce such a spectrum is the presence of multiple gas components at different velocities, perhaps from an embedded binary system. In this case, the NH$_3$(6, 6) line has to have exactly the right optical depth to sample specifically these two gas parcels.

Another way to get such a double-peaked profile is rotation of a central circum-protostellar disk. Such a double horn spectral profile is expected if one observed such a disk in a near-edge-on configuration where the gain path of the red-receding and blue-approaching disk components are long enough to produce enough emission at the corresponding velocities (Beckwith & Sargent 1993). The fact that we do not see such a double-peaked profile in the NH$_3$(5, 5) line may be explained by a
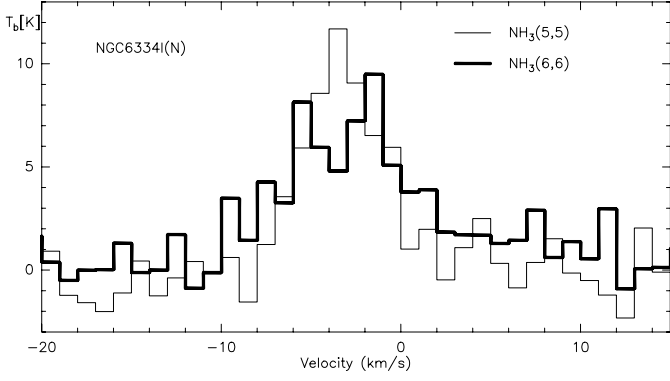
Fig. 8. NH$_3$(5, 5) and (6, 6) spectra in NGC 6334I(N) extracted after imaging toward the their peak positions associated with the main mm continuum peak. The spectral resolution is 1 km s^{-1} and the spatial resolution $2.8 \times 2.4''$.

larger optical depth of this line which hence may not trace the inner disk structure at all. Double-peaked profiles of some maser emission features were interpreted in the past sometimes in the framework of rotation in a Keplerian disk (e.g., Cesaroni 1990; Ponomarev et al. 1994). However, the emission observed in the NH$_3$(6, 6) line toward NGC 6334I(N) does not appear maser-like and is likely of thermal nature.

With the current data, we cannot distinguish whether the double-peaked spectrum is produced by multiple, isolated gas parcels or by a contiguous structure like a rotating disk. Nevertheless, let us follow the disk proposal for a moment: assuming equilibrium between the centrifugal and gravitational force in an edge-on disk (inclination angle $i = 90°$), the radius of such a disk would be:

$$r[\text{AU}] = \frac{M[M_\odot]}{1.13 \times 10^{-3}\, \Delta v^2 [\text{km s}^{-1}]} \sin^2 i$$

With a separation Δv between the two NH$_3$(6, 6) peaks of 4 km s^{-1} and an approximate enclosed mass of 20 $M_\odot$ estimated from the mm continuum data (Hunter et al. 2006), the approximate diameter of this tentative disk-like structure is 2200 AU, corresponding to an angular size of $1.3''$.

To discriminate between the different possibilities, higher spatial resolution observations of the NH$_3$(6, 6) line will be required to resolve and image this potential massive accretion disk in more detail. Furthermore, one can look for even higher excitation NH$_3$ lines: In the disk scenario, one would expect line profiles similar to that observed in the (6, 6) line, but with a larger velocity separation since the warmer gas would be found at smaller disk radii in a centrally heated Keplerian disk. In a multi-component scenario, different line opacities could result in the higher energy transitions sampling different gas components, which would produce different line profiles for the higher transitions.

5. Conclusions and summary

High spatial resolution imaging of the highly excited NH$_3$ inversion lines (3, 3) to (6, 6) revealed warm gas components toward both of the twin cores NGC 6334I and I(N). This is particularly surprising for NGC 6334I(N) because this region was always considered to be the prototypical massive cold core. While NGC 6334I(N) is still in a very young evolutionary stage it has already formed at least one central massive protostar that has begun to heat up its surrounding environment. For the well-known

hot core NGC 6334I, the detection of the higher excitation lines is less surprising. However, the optical depths of the NH$_3$(1, 1) to (4, 4) are so high in both regions that the hyperfine spectra are difficult to fit. In NGC 6334I, one can use the (5, 5) and (6, 6) lines to estimate rotational temperatures toward the mm continuum sources mm1 and mm2 of 86 ± 20 and 67 ± 20 K, respectively. However, since these two inversion lines are from different NH$_3$ species (para- and ortho-NH$_3$), such rotational temperature estimates have to been taken cautiously. We also tried to estimate the opacities, and from that the rotational temperatures and column densities, of the NH$_3$(3, 3) and (4, 4) lines using the ratios between the main and satellite components of their spectra. While these estimates qualitatively confirm the previous estimates they also show the limitations and associated errors of the NH$_3$ analysis in regions of that high column densities and temperatures. Toward NGC 6334I(N), a rotational temperature estimate is not possible because the NH$_3$(6, 6) spectrum is double-peaked and hence does not allow reasonable line fits. Therefore, we only conclude that both regions harbor dense cores with kinetic temperatures >100 K. For better temperature estimates, one has either to observe optically thin isotopologues like ^{15}NH$_3$, or go to even higher excitation inversion transitions like the NH$_3$(7, 7) and NH$_3$(8, 8) lines, or try to model the spectra with more sophisticated radiative transfer methods. A different approach is to study other molecules with different abundances and energy levels above ground. Many such molecules have a rich line spectrum in the (sub)mm wavelength windows, and a complementary study with the Submillimeter Array is currently in progress (Hunter et al. in prep.).

We confirm the previous detection of the NH$_3$(3, 3) maser toward the two outflow lobes in NGC 6334I. The north-eastern NH$_3$(3, 3) maser morphology even resembles the shape of typical outflow bow-shocks. Furthermore, we report the first detection of NH$_3$(6, 6) maser emission toward the central cores in NGC 6334I. The main NH$_3$(6, 6) maser peak is associated with the mm peak 2 and elongated along the outflow axis. Therefore, we suggest that the strongest line and continuum source in this region, mm1, is not the driving source of the prominent molecular outflow, but rather the weaker sub-source, mm2.

While past observations revealed strong line emission on large-spatial scales toward NGC 6334I(N), no previous observations detected compact gas cores at the center of the region. Observations of the highly excited NH$_3$(4, 4) to (6, 6) lines for the first time detect compact warm gas emission from the central main mm peak. The observed line with the highest energy above ground, NH$_3$(6, 6), is not single-peaked toward that main mm continuum core, but it shows a double-horn profile. With the current data we cannot differentiate whether this double-horn line profile is caused by multiple gas components along the line of sight (maybe even a binary system) or whether it may be the signature of a potentially underlying massive accretion disk. Higher spatial resolution observations of the NH$_3$(6, 6) or even higher excited lines that can resolve the sub-structure of this core are required to solve this question.

References

Bachiller, R., & Cernicharo, J. 1990, A&A, 239, 276
Beckwith, S. V. W., & Sargent, A. I. 1993, ApJ, 402, 280

Beuther, H., Thorwirth, S., Zhang, Q., et al. 2005, ApJ, 627, 834
Brooks, K. J., & Whiteoak, J. B. 2001, MNRAS, 320, 465
Carral, P., Kurtz, S. E., Rodríguez, L. F., et al. 2002, AJ, 123, 2574
Caswell, J. L. 1997, MNRAS, 289, 203
Cesaroni, R. 1990, A&A, 233, 513
Coudert, L. H., & Roueff, E. 2006, A&A, 449, 855
Davis, C. J., & Eisloeffel, J. 1995, A&A, 300, 851
De Buizer, J. M., Radomski, J. T., Piña, R. K., & Telesco, C. M. 2002, ApJ, 580, 305
de Pree, C. G., Rodriguez, L. F., Dickel, H. R., & Goss, W. M. 1995, ApJ, 447, 220
Forster, J. R., & Caswell, J. L. 1989, A&A, 213, 339
Gaume, R. A., & Mutel, R. L. 1987, ApJS, 65, 193
Gezari, D. Y. 1982, ApJ, 259, L29
Ho, P. T. P., & Townes, C. H. 1983, ARA&A, 21, 239
Hunter, T. R., Brogan, C. L., Megeath, S. T., et al. 2006, ApJ, 649, 888
Kogan, L., & Slysh, V. 1998, ApJ, 497, 800
Kraemer, K. E., & Jackson, J. M. 1995, ApJ, 439, L9
Leurini, S., Schilke, P., Parise, B., et al. 2006, A&A, 454, L83
Loughran, L., McBreen, B., Fazio, G. G., et al. 1986, ApJ, 303, 629
McBreen, B., Fazio, G. G., Stier, M., & Wright, E. L. 1979, ApJ, 232, L183
McCutcheon, W. H., Sandell, G., Matthews, H. E., et al. 2000, MNRAS, 316, 152

Megeath, S. T., & Tieftrunk, A. R. 1999, ApJ, 526, L113
Moran, J. M., & Rodríguez, L. F. 1980, ApJ, 236, L159
Myers, P. C., Mardones, D., Tafalla, M., Williams, J. P., & Wilner, D. J. 1996, ApJ, 465, L133
Neckel, T. 1978, A&A, 69, 51
Norris, R. P., Whiteoak, J. B., Caswell, J. L., Wieringa, M. H., & Gough, R. G. 1993, ApJ, 412, 222
Persi, P., Roth, M., Tapia, M., et al. 1996, A&A, 307, 591
Persi, P., Tapia, M., Roth, M., Gómez, M., & Marenzi, A. R. 2005, in IAU Symp. 227, ed. R. Cesaroni, M. Felli, E. Churchwell, & M. Walmsley, 291
Ponomarev, V. O., Smith, H. A., & Strelnitski, V. S. 1994, ApJ, 424, 976
Rodríguez, L. F., Canto, J., & Moran, J. M. 1982, ApJ, 255, 103
Sandell, G. 2000, A&A, 358, 242
Schilke, P., Comito, C., Thorwirth, S., et al. 2006, A&A, 454, L41
Sollins, P. K., & Megeath, S. T. 2004, AJ, 128, 2374
Straw, S. M., & Hyland, A. R. 1989, ApJ, 340, 318
Tapia, M., Persi, P., & Roth, M. 1996, A&A, 316, 102
Thorwirth, S., Winnewisser, G., Megeath, S. T., & Tieftrunk, A. R. 2003, in Galactic Star Formation Across the Stellar Mass Spectrum, ASP Conf. Ser., 287, 257
van Dishoeck, E. F., & Blake, G. A. 1998, ARA&A, 36, 317
Walsh, A. J., Burton, M. G., Hyland, A. R., & Robinson, G. 1998, MNRAS, 301, 640